

LETTER

Electron-transfer-induced metallic electronic states in a H/Fe₃O₄(001) film subsurface

To cite this article: Satoshi Hiura *et al* 2019 *Appl. Phys. Express* **12** 055502

View the [article online](#) for updates and enhancements.

You may also like

- [Direct observation of subsurface charge ordering in Fe₃O₄\(001\) by scanning tunneling microscopy/spectroscopy](#)
Satoshi Hiura, Akira Ikeuchi, Masafumi Jochi *et al.*
- [Intrinsic stability of ferroelectric and piezoelectric properties of epitaxial PbZr_{0.45}Ti_{0.55}O₃ thin films on silicon in relation to grain tilt](#)
Evert P Houwman, Minh D Nguyen, Matthijn Dekkers *et al.*
- [Highly Tunable Perpendicular Magnetic Anisotropy and Anisotropic Magnetoresistance in Ru-Doped La_{0.67}Sr_{0.33}MnO₃ Epitaxial Films](#)
Enda Hua, , Kunjie Dai *et al.*



Electron-transfer-induced metallic electronic states in a H/Fe₃O₄(001) film subsurface

Satoshi Hiura^{*}, Agus Subagyo, Akihiro Murayama, and Kazuhisa Sueoka

Graduate School of Information Science and Technology, Hokkaido University, Sapporo 060-0814, Japan

^{*}E-mail: hiura@ist.hokudai.ac.jp

Received February 26, 2019; revised March 13, 2019; accepted March 18, 2019; published online April 5, 2019

We investigate the local electronic properties of Fe atoms in a H/Fe₃O₄(001) film subsurface using scanning tunneling microscopy/spectroscopy (STS). Local barrier height measurements show a H-adsorption-induced reduction of the local work function, indicating electron transfer from H to surface atoms. The STS results and high-resolution spatial mapping of the occupied density of states near the Fermi level reveal that subsurface Fe atoms located beneath a OH group exhibit a metallic electronic state, different from the semiconducting state for intrinsic subsurface Fe atoms. These results can be explained by considering the extension of electron transfer to the subsurface layer.

© 2019 The Japan Society of Applied Physics

Supplementary material for this article is available [online](#)

Magnetite (Fe₃O₄) is a magnetic material that exhibits fascinating properties for spintronic device applications, such as theoretically predicted half-metallicity and a high Curie temperature of 858 K.^{1,2)} Although these features have led to the development of magnetic tunnel junction devices that use Fe₃O₄ films as ferromagnetic electrodes, these magnetic devices display poor performance^{3,4)} because of the reduced electron-spin polarization at the interface.⁵⁾ In fact, the topmost surfaces of clean Fe₃O₄(001) exhibit only -5% electron-spin polarization near the Fermi level.^{6,7)} Thus, novel methods or structural designs are required to greatly enhance the surface and interface electron-spin polarization.

Recently, experimental and theoretical investigations have shown that the adsorption of various atoms (H,^{6–9)} C,¹⁰⁾ and B¹¹⁾ and molecules (C₆H₆⁷⁾ and C₆₀¹²⁾ on the Fe₃O₄(001) surface produces a significant enhancement in the surface electron-spin polarization. In most cases, density functional theory (DFT) calculations predict that electron transfer between adsorbed atoms (molecules) and surface atoms can significantly modify the surface electronic states.^{8–12)} To reveal this electron transfer mechanism experimentally, an understanding of the atomic-scale work function (WF) and electronic properties is essential. Scanning tunneling microscopy/spectroscopy (STM/STS) methods are powerful tools for obtaining surface structural and electronic properties at atomic scales. The effect of H atoms on surface Fe electronic states in Fe₃O₄(001) film has previously been explored using STM/STS.^{13,14)} DFT calculations predict that the adsorption of H atoms on the Fe₃O₄(001) surface modifies both the surface and subsurface Fe electronic states.^{8,9)} However, the modification of the subsurface Fe electronic properties induced by H adsorption has not been experimentally explored. Further investigation of the changes in subsurface electronic properties at the atomic-scale would advance our understanding of the interactions between adsorbed H and both the surface and subsurface atoms, and may provide information on the origin of the enhanced electron-spin polarization of H/Fe₃O₄(001) surfaces. Moreover, these findings could offer a new pathway toward interface spin engineering for spintronic device applications.

In this study, we utilize STM/STS to investigate the change in the local WF induced by H adsorption and the

local electronic states of subsurface Fe atoms located beneath an OH group. H adsorption on the surface is realized by the dissociative adsorption of ultra-high vacuum (UHV) residual gases such as H₂O, which is the same as the previous reports.^{13–15)} This study focuses on occupied electronic states just below the Fermi level, corresponding to Fe²⁺ cations. These occupied states are investigated by STS and by spatial differential conductance (dI/dV) mapping using the multipass scanning method.¹⁶⁾

All experiments were performed in an UHV system (base pressure $<10^{-10}$ mbar) composed of a preparation chamber for sample preparation and an analysis chamber for X-ray photoelectron spectroscopy (XPS) and STM/STS. Fe₃O₄(001) films of 20 nm thickness were epitaxially grown on single-crystal MgO(001) substrates by electron beam deposition of Fe in oxygen.^{13–15,17)} The film stoichiometry and its surface chemical structures were confirmed by XPS. The XPS spectra showed a good Fe₃O₄ stoichiometry, and demonstrated the presence of surface OH groups, as discussed in Fig. 1(a). STM/STS measurements were performed at room temperature using tungsten tips. All STM images were acquired in the constant-current mode. A bias voltage was applied to the sample with respect to the grounded tip. STS measurements were performed with the feedback loop turned off. The dI/dV signals were obtained using a standard lock-in technique with a 20 mV bias modulation at 5.24 kHz.

Figure 1(a) shows the Shirley background-subtracted O 1s XPS spectrum acquired from the freshly prepared Fe₃O₄(001) film, which is decomposed into two components. The lower energy peak at 530.2 eV is assigned to the oxygen in Fe₃O₄.¹⁸⁾ The higher-energy small peak shifted by +1.3 eV is attributed to the OH group,¹⁹⁾ which is due to no detection of carbonyl groups from C 1s XPS spectra. This XPS result demonstrates the presence of surface OH groups. Figure 1(b) shows an STM image of the as-grown Fe₃O₄(001) film surface. Atomic rows running along the [110] direction are clearly visible. The averaged distances between neighboring rows and between neighboring atoms within each row are ~ 0.6 and ~ 0.3 nm, respectively.^{20,21)} Because these atom periodicities correspond to those of the Fe atoms in the B-terminated Fe₃O₄(001) surface [denoted as Fe_B(S) in Fig. 1(d)], the observed atoms should represent single Fe_B(S) atoms. Moreover, the STM image exhibits undulating

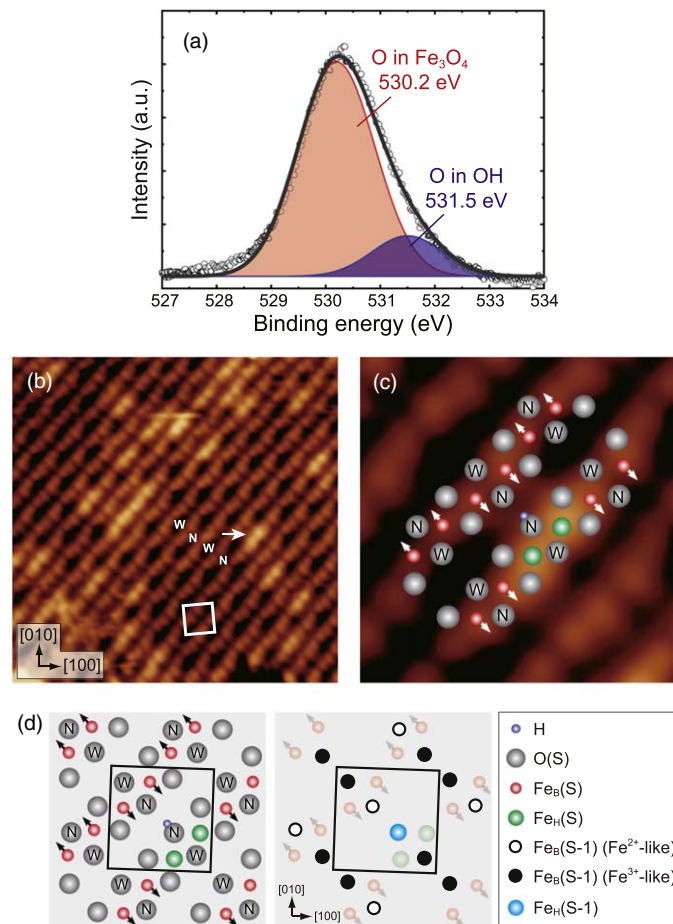


Fig. 1. (Color online) (a) O 1s XPS spectrum acquired from the freshly prepared $\text{Fe}_3\text{O}_4(001)$ film using Mg $K\alpha$ radiation. The spectrum is decomposed into two components, as discussed in the text. (b) Overview STM image of the $\text{H}/\text{Fe}_3\text{O}_4(001)$ film surface ($11.0 \times 11.0 \text{ nm}^2$, $V_s = +1.0 \text{ V}$, and $I_t = 0.3 \text{ nA}$). The displacement of $\text{Fe}_B(\text{S})$ atoms generates nonequivalent narrow (N) and wide (W) sections. The white arrow shows $\text{Fe}_H(\text{S})$ atoms with an OH group neighbor. (c) High-resolution STM image ($2.5 \times 2.5 \text{ nm}^2$, $V_s = +1.0 \text{ V}$, and $I_t = 0.3 \text{ nA}$). The white arrows indicate the directions of the displacements of $\text{Fe}_B(\text{S})$ atoms. (d) Model of (left) B-terminated surface structure and (right) subsurface charge-ordered structure of $\text{Fe}_3\text{O}_4(001)$ with one OH group within the unit cell.

$\text{Fe}_B(\text{S})$ rows. The wave-like structures are derived from a subtle lattice distortion whereby alternate pairs of $\text{Fe}_B(\text{S})$ atoms relax laterally in opposite directions perpendicular to the row,²²⁾ as indicated by the white arrows in Fig. 1(c). These small displacements of the $\text{Fe}_B(\text{S})$ atoms generate two nonequivalent “narrow” and “wide” sections [indicated by the letters N and W in Fig. 1(b)], composing the $(\sqrt{2} \times \sqrt{2})R45^\circ$ unit cell marked with the white square in Fig. 1(b). Following a previous STM report,²³⁾ we denote the two nonequivalent O(S) atoms produced by the distortion as O_N and O_W .^{13–15)}

There are many bright protrusions situated at $\text{Fe}_B(\text{S})$ sites in the STM image, as indicated by the white arrow in Fig. 1(b). These bright protrusions are surface Fe_B atoms with an OH group neighbor [denoted as $\text{Fe}_H(\text{S})$ in Fig. 1(d)]. The electronic states of these atoms are significantly modified by the neighboring OH groups.^{13–15,23)} Figure 1(c) shows a high-resolution STM image of an area containing $\text{Fe}_H(\text{S})$ atoms. Two neighboring $\text{Fe}_H(\text{S})$ atoms are observed as bright protrusions. Previous STM imaging of the $\text{H}/\text{Fe}_3\text{O}_4(001)$ surface revealed that H atoms bonded to O_N sites modify the local electronic states in the neighboring two- $\text{Fe}_B(\text{S})$ -atom pair.²³⁾

Previous STS results acquired on $\text{Fe}_H(\text{S})$ sites revealed a state 0.2 eV below the Fermi level.¹³⁾ This result indicates

that the surface is reduced by H adsorption, i.e., the surface $\text{Fe}_B(\text{S})$ atoms change from Fe^{3+} to Fe^{2+} -like cations. The change in the surface Fe electronic states is theoretically predicted to originate from electron transfer between H atoms and $\text{Fe}_B(\text{S})$ atoms via O(S) atoms.⁹⁾ The important parameter for discussing electron transfer between adsorbates and surfaces is the WF. In this study, WFs on $\text{Fe}_B(\text{S})$ and $\text{Fe}_H(\text{S})$ sites were investigated to gain an insight into the electron transfer phenomenon. An efficient method of determining the local WF is to measure the local barrier height (LBH). The LBH measured with STM is defined as^{24–26)}

$$\Phi \cong 0.952 \left(\frac{d}{dz} \ln I \right)^2,$$

where I , z , and Φ are the tunneling current, tip-sample distance, and the measured LBH. Note that the measured LBH is not the WF of the sample, but the mean value of the WF of the tip, Φ_T , and that of the sample, Φ_S , i.e., $\Phi = (\Phi_T + \Phi_S)/2$. Using this formula, the LBH can be calculated from the measured I - z curves. Figure 2(a) shows typical I - z curves in logarithmic coordinates obtained for $\text{Fe}_B(\text{S})$ and $\text{Fe}_H(\text{S})$ sites at a set point of $V_s = +1.2 \text{ V}$ and $I_t = 0.6 \text{ nA}$. Both curves exhibit exponential decay features with increasing tip-sample distance. The LBH on the $\text{Fe}_B(\text{S})$ site is $4.89 \pm 0.03 \text{ eV}$, whereas the $\text{Fe}_H(\text{S})$ site has a much lower

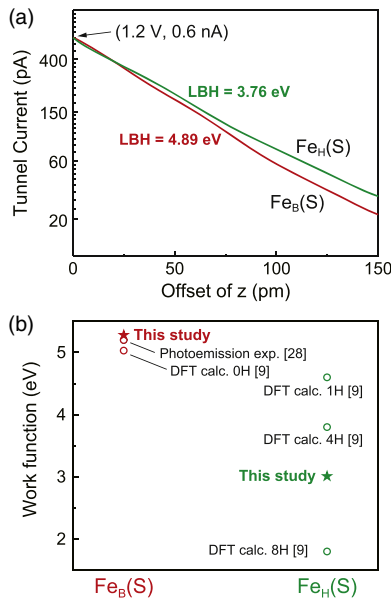


Fig. 2. (Color online) (a) Averaged I - z curves obtained on $\text{Fe}_B(\text{S})$ and $\text{Fe}_H(\text{S})$ sites. z is the tip-sample distance and is set as a reference point ($z = 0$ pm) at a set point of $V_s = +1.2$ V and $I_t = 0.6$ nA. (b) Work functions on $\text{Fe}_B(\text{S})$ and $\text{Fe}_H(\text{S})$ sites numerically calculated from the I - z curves. Previous theoretical and experimental results of work functions on $\text{Fe}_3\text{O}_4(001)$ and $\text{H}/\text{Fe}_3\text{O}_4(001)$ surfaces are also plotted.

LBH value of 3.76 ± 0.02 eV. In this case, the WF value on the $\text{Fe}_B(\text{S})$ [$\text{Fe}_H(\text{S})$] site can be estimated as 5.28 ± 0.06 eV (3.01 ± 0.04 eV) by assuming $\Phi_T = 4.5$ eV for tungsten in STM studies,²⁷⁾ as shown in Fig. 2(b). This WF value of 5.28 eV for the $\text{Fe}_B(\text{S})$ site agrees well with the value of 5.20 eV measured in photoemission experiments²⁸⁾ and the calculated values of 5.32²²⁾ and 5.03 eV⁹⁾ for the $\text{Fe}_3\text{O}_4(001)$ surface. However, the WF value of 3.01 eV for the $\text{Fe}_H(\text{S})$ site is much smaller than the calculated values of 3.8–4.6 eV for $\text{H}/\text{Fe}_3\text{O}_4(001)$ surfaces with one to four hydrogen atoms per unit cell.⁹⁾ In addition, this WF value of 3.01 eV is larger than the 1.8 eV of $\text{H}/\text{Fe}_3\text{O}_4(001)$ surfaces with eight hydrogen atoms per unit cell,⁹⁾ where H atoms are bonded to all surface O atoms. The difference between this study and previous theoretical examinations may be the result of the different atomic-scale WFs obtained by STM and DFT. The lower WF value of the $\text{Fe}_H(\text{S})$ site clearly indicates the hydrogen-induced reduction of the WF of the $\text{Fe}_3\text{O}_4(001)$ surface. In addition, these results demonstrate the electron transfer from H atoms to the $\text{Fe}_3\text{O}_4(001)$ surface, and hence the dipole moment of the surface OH groups.⁹⁾

We next focus on the effect of H atoms on subsurface Fe atoms [denoted as $\text{Fe}_B(\text{S}-1)$ in Fig. 1(d)]. Recent STM/STS studies of a UHV-prepared $\text{Fe}_3\text{O}_4(001)$ film revealed charge ordering of $\text{Fe}^{2+}-\text{Fe}^{2+}$ and $\text{Fe}^{3+}-\text{Fe}^{3+}$ dimers in the subsurface layer.²⁰⁾ In this study, we investigated the local electronic properties of subsurface Fe atoms located beneath an OH group [denoted as $\text{Fe}_H(\text{S}-1)$ in Fig. 1(d)] to reveal the effect of H atoms on Fe electronic states in the subsurface layer where the abovementioned charge ordering occurs. Figure 3 shows I - V curves obtained for $\text{Fe}_B(\text{S}-1)$ and $\text{Fe}_H(\text{S}-1)$ sites. Here, $\text{Fe}_H(\text{S}-1)$ atoms are defined as subsurface Fe_B atoms located beneath surface O_NH groups, as H atoms can only bond to O_N sites.^{14,15)} We also define the $\text{Fe}_B(\text{S}-1)$ atoms as subsurface Fe_B atoms located beneath O_N

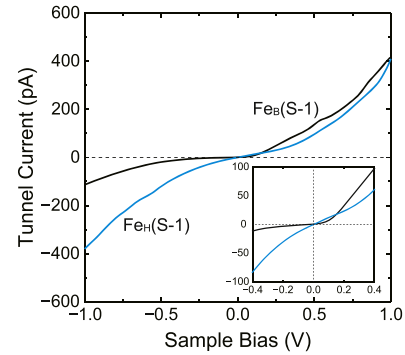


Fig. 3. (Color online) I - V curves obtained on $\text{Fe}_B(\text{S}-1)$ and $\text{Fe}_H(\text{S}-1)$ sites with a z offset of 100 pm toward the surface with respect to the original set point of $V_s = +1.0$ V and $I_t = 0.2$ nA. The inset shows the region around $V_s = 0$ V.

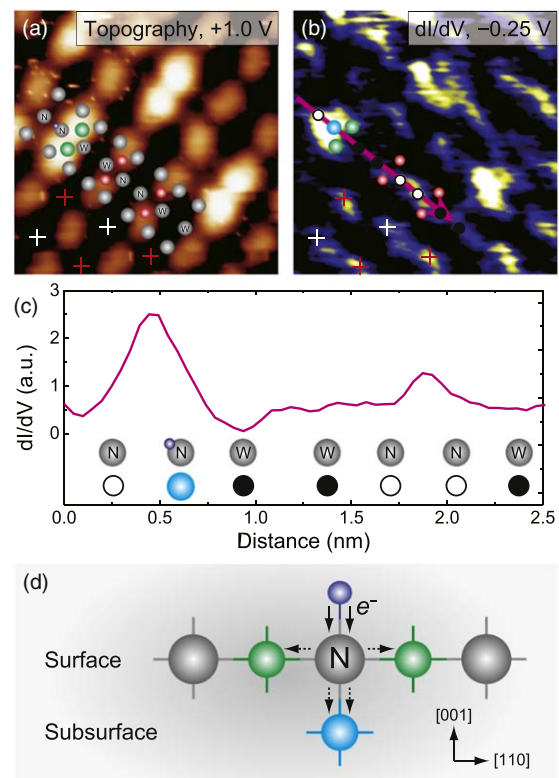


Fig. 4. (Color online) (a) High-resolution STM image (3.3×3.3 nm², $V_s = +1.0$ V, and $I_t = 0.3$ nA) and (b) dI/dV image ($V_s = -0.25$ V). The red and white crosses indicate the narrow and wide sections, respectively. (c) Cross-sectional line profile taken along the arrow in (b). Atomic arrangement is shown at the bottom. (d) Atomic arrangement model of an $\text{H}/\text{Fe}_3\text{O}_4(001)$ surface and subsurface. The arrows indicate the directions of electron flow. The color coding of the atoms corresponds to the scheme in Fig. 1(d).

atoms. These I - V curves were obtained with a z offset of 100 pm toward the surface with respect to the original set point of $V_s = +1.0$ V and $I_t = 0.2$ nA so that the subsurface electronic states could be effectively detected. $\text{Fe}_H(\text{S}-1)$ atoms have a much higher occupied density of states (DOS) below the Fermi level, resulting in a larger tunneling current at negative bias voltages. Note that $\text{Fe}_H(\text{S}-1)$ atoms have a visible DOS around the Fermi level, indicating a metallic nature with respect to the semiconducting nature of $\text{Fe}_B(\text{S}-1)$ atoms, as clearly seen in the inset. We also performed dI/dV mapping of the $\text{H}/\text{Fe}_3\text{O}_4(001)$ film surface

to further understand the subsurface electronic structure. Figures 4(a) and 4(b) show a set of images acquired using the previously described multipass scanning method.¹⁶⁾ The STM [Fig. 4(a)] and dI/dV [Fig. 4(b)] images were obtained at bias voltages of +1.0 V and -0.25 V, respectively. The identical electronic structures were reproducibly obtained on different samples using tips that were sufficiently treated (see the online supplementary data available online at stacks.iop.org/APEX/12/055502/mmedia). Comparing these images suggests that two types of DOS distributions are observed between the $\text{Fe}_B(\text{S})$ rows. The higher (lower) DOS is observed at the narrow (wide) section, where $\text{Fe}^{2+}\text{-Fe}^{2+}$ ($\text{Fe}^{3+}\text{-Fe}^{3+}$) dimers are periodically arranged according to the subsurface charge ordering model shown in Fig. 1(d).

Figures 4(a) and 4(b) enable a detailed understanding of the local electronic properties of Fe atoms in both the $\text{Fe}_3\text{O}_4(001)$ film surface and subsurface. In the dI/dV image, pairs of $\text{Fe}_H(\text{S})$ atoms exhibit a much higher DOS than $\text{Fe}_B(\text{S})$ atoms, which agrees with the STS result.^{13,14)} Moreover, the dI/dV image shows that the highest DOS occurs at the narrow section with an OH group. Figure 4(c) shows the cross-sectional line profile of the dI/dV image taken along the arrow indicated in Fig. 4(b). Given that DFT calculations predict the DOS of O(S) atoms to be almost zero near the Fermi level,²⁹⁾ this highest DOS should reflect the greater reduction in subsurface Fe atoms than in $\text{Fe}_B(\text{S}-1)$ atoms. This metallization of subsurface Fe atoms induced by H adsorption is similar to the DFT result for the $\text{C}/\text{Fe}_3\text{O}_4(001)$ surface,¹⁰⁾ which showed a metallic state in subsurface Fe atoms and a semiconducting state in surface Fe atoms. A DFT study of $\text{H}/\text{Fe}_3\text{O}_4(001)$ surfaces also predicted that the saturation of O(S) dangling bonds by H adsorption induces small but evident electron redistribution among atoms at the topmost surface and at the subsurface layer.⁸⁾ This electron donation means that $\text{Fe}_H(\text{S}-1)$ atoms gain electrons from adsorbed H atoms through the saturation of O(S) dangling bonds, and the $\text{Fe}_H(\text{S}-1)$ atoms are reduced to Fe^{2+} . The extension of this electron transfer to the subsurface layer occurs in our $\text{H}/\text{Fe}_3\text{O}_4(001)$ film. Figure 4(b) also shows that the highest DOS is distributed to the $\text{Fe}_B(\text{S}-1)$ atoms in opposite rows. Because the strong tilt of H atoms from an initial on-top position results in OH bonds between H atoms and O_N atoms in opposite rows,^{9,10)} extra electrons should be donated to the $\text{Fe}_B(\text{S}-1)$ atoms in the opposite rows.

Judging from these results, both the surface and subsurface Fe atoms should gain electrons from H atoms via O(S) atoms, as illustrated in Fig. 4(d). This electron donation enhances the occupied DOS near the Fermi level of both surface and subsurface Fe atoms. As the electronic states near the Fermi level of Fe_B atoms are dominated by spin-down electronic states,^{28,30,31)} the enhanced DOS would be caused by the gain of spin-down electrons from H atoms. Therefore, adsorption of H atoms on the $\text{Fe}_3\text{O}_4(001)$ film surface can enhance the electron-spin polarization of not only the topmost surface, but also the underlying subsurface. These findings regarding the modification of subsurface Fe electronic states induced by H adsorption will play a significant role in designing interface electronic structures and modifying them for effective spin-polarized charge transport in organic spintronic devices.

In summary, local WFs on surface Fe sites and the local electronic properties of Fe atoms in $\text{H}/\text{Fe}_3\text{O}_4(001)$ film subsurface were investigated by LBH and STM/STS measurements. The LBH results showed a reduction in the local WF induced by H adsorption. The WF value obtained on $\text{Fe}_B(\text{S})$ sites was in good agreement with previous theoretical and experimental values for clean $\text{Fe}_3\text{O}_4(001)$ surfaces. The STS results revealed that subsurface Fe atoms located beneath an OH group exhibit a metallic nature. These Fe electronic structures were clearly observed by spatial dI/dV mapping of the occupied states just below the Fermi level. These combinations of LBH and STM/STS measurements demonstrated that not only the surface Fe atoms, but also the subsurface ones, can gain electrons from H atoms through electron donation and redistribution processes via the saturation of O(S) dangling bonds.

Acknowledgments This work was supported by JSPS KAKENHI Grant No. JP17H06482, and was partially supported by JSPS KAKENHI Grant No. JP16H06359. Experiments were conducted at Hokkaido University supported by the Nanotechnology Platform Program of the Ministry of Education, Culture, Sports, Science and Technology (MEXT), Japan.

ORCID iDs Satoshi Hiura  <https://orcid.org/0000-0002-0710-2777>

- 1) A. Yanase and N. Hamada, *J. Phys. Soc. Jpn.* **68**, 1607 (1999).
- 2) Z. Zhang and S. Satpathy, *Phys. Rev. B* **44**, 13319 (1991).
- 3) T. Kado, *Appl. Phys. Lett.* **92**, 092502 (2008).
- 4) M. Opel, *J. Phys. D: Appl. Phys.* **45**, 033001 (2012).
- 5) A. M. Bataille, A. Tagliaferri, S. Gota, C. de Nadaï, J.-B. Moussy, M.-J. Guittet, K. Bouzehouane, F. Petroff, M. Gautier-Soyer, and N. B. Brookes, *Phys. Rev. B* **73**, 172201 (2006).
- 6) M. Kurahashi, X. Sun, and Y. Yamauchi, *Phys. Rev. B* **81**, 193402 (2010).
- 7) A. Pratt, M. Kurahashi, X. Sun, and Y. Yamauchi, *J. Phys. D: Appl. Phys.* **44**, 064010 (2011).
- 8) X. Sun, M. Kurahashi, A. Pratt, and Y. Yamauchi, *Surf. Sci.* **605**, 1067 (2011).
- 9) N. Mulakaluri and R. Pentcheva, *J. Phys. Chem. C* **116**, 16447 (2012).
- 10) X. Sun, S. D. Li, B. Wang, M. Kurahashi, A. Pratt, and Y. Yamauchi, *Phys. Chem. Chem. Phys.* **16**, 95 (2014).
- 11) X. Sun, A. Pratt, and Y. Yamauchi, *Phys. Chem. Chem. Phys.* **17**, 15386 (2015).
- 12) P. K. J. Wong, W. Zhang, G. van der Laan, and M. P. de Jong, *Org. Electron.* **29**, 39 (2016).
- 13) S. Hiura, A. Ikeuchi, S. Shirini, A. Subagy, and K. Sueoka, *Phys. Rev. B* **91**, 205411 (2015).
- 14) S. Hiura, A. Ikeuchi, S. Shirini, A. Subagy, and K. Sueoka, *Jpn. J. Appl. Phys.* **54**, 08LB02 (2015).
- 15) S. Hiura, A. Ikeuchi, S. Shirini, A. Subagy, and K. Sueoka, *e-J. Surf. Sci. Nanotech.* **12**, 26 (2014).
- 16) N. Ishida, M. Jo, T. Mano, Y. Sakuma, T. Noda, and D. Fujita, *Nanoscale* **7**, 16773 (2015).
- 17) A. Subagy and K. Sueoka, *Jpn. J. Appl. Phys.* **44**, 5447 (2005).
- 18) V. Chandra, J. Park, Y. Chun, J. W. Lee, I. C. Hwang, and K. S. Kim, *ACS Nano* **4**, 3979 (2010).
- 19) T. Kendelewicz, S. Kaya, J. T. Newberg, H. Bluhm, N. Mulakaluri, W. Moritz, M. Scheffler, A. Nilsson, R. Pentcheva, and G. E. Brown Jr., *J. Phys. Chem. C* **117**, 2719 (2013).
- 20) S. Hiura, A. Ikeuchi, M. Jochi, R. Yamazaki, S. Takahashi, A. Subagy, A. Murayama, and K. Sueoka, *Appl. Phys. Express* **10**, 045701 (2017).
- 21) B. Stanka, W. Hebenstreit, U. Diebold, and S. A. Chambers, *Surf. Sci.* **448**, 49 (2000).
- 22) R. Pentcheva, F. Wendler, H. L. Meyerheim, W. Moritz, N. Jedrecy, and M. Scheffler, *Phys. Rev. Lett.* **94**, 126101 (2005).
- 23) G. S. Parkinson, Z. Novotný, P. Jacobson, M. Schmid, and U. Diebold, *J. Am. Chem. Soc.* **133**, 12650 (2011).
- 24) G. Binnig, H. Rohrer, C. Gerber, and E. Weibel, *Appl. Phys. Lett.* **40**, 178 (1982).
- 25) G. Binnig, N. Garcia, H. Rohrer, J. M. Soler, and F. Flores, *Phys. Rev. B* **30**, 4816 (1984).

- 26) W. Feng, S. Lei, Q. Li, and A. Zhao, *J. Phys. Chem. C* **115**, 24858 (2011).
- 27) A. P. Wijnheijmer, J. K. Garleff, M. A. V. D Heijden, and P. M. Koenraad, *J. Vac. Sci. Technol. B* **28**, 21086 (2010).
- 28) M. Fonin, R. Pentcheva, Y. S. Dedkov, M. Sperlich, D. V. Vyalikh, M. Scheffler, U. Rüdiger, and G. Güntherodt, *Phys. Rev. B* **72**, 104436 (2005).
- 29) I. Bernal-Villamil and S. Gallego, *J. Phys.: Condens. Matter* **27**, 012001 (2015).
- 30) I. V. Shvets, G. Mariotto, K. Jordan, N. Berdunov, R. Kantor, and S. Murphy, *Phys. Rev. B* **70**, 155406 (2004).
- 31) K. Jordan, A. Cazacu, G. Manai, S. F. Ceballos, S. Murphy, and I. V. Shvets, *Phys. Rev. B* **74**, 085416 (2006).